The Study of the Silicon Detector Response for p-Carbon Polarization Measurements at RHIC

D. Kalinkin[*1] and D. Smirnov[†2]

[1]Institute for Theoretical and Experimental Physics
[2]Brookhaven National Laboratory

August 31, 2014

Abstract

At the Relativistic Heavy Ion Collider (RHIC) measurements of the proton beam polarization are conducted by inserting an ultra thin carbon ribbon in the beam and registering the scattered carbon ions with silicon detectors. The polarization value reported by the proton-carbon polarimeters strongly depends on the correct measurement of the energy deposited in the detectors by the recoil products. In this note we present a study of the response of the silicon detectors to α-particles employed to calibrate the detectors.

1 Motivation

The RHIC polarimetry is based on the measurement of the recoil products from elastic scattering of the proton beam on a fixed target in the Coulomb nuclear interference (CNI) energy regime. In this study we focus on the four p-Carbon polarimeters with ultra thin carbon targets which can be moved through the beam. In the current setup the polarization of each proton beam can be measured independently by two p-Carbon polarimeters installed in the "yellow" and "blue" accelerator rings.

During the 2013 run we observed significant changes in the gain in some of the silicon detectors. This change of $\lesssim 20$ % is worrisome and may cause significant systematic change in the reported polarization values due to a steep slope in the p-Carbon analyzing power within the energy range of interest.

2 Measurement and Results

The detectors produced by the BNL instrumentation group have 12 one-millimeter silicon strips operating under the nominal bias voltage of 110 V. The detector gains are normally monitored by taking calibration runs when there is no beam in the machine. Starting April 3, 2013 the calibration runs were taken automatically at the end of every RHIC store immediately after the beam dump. This approach allowed us to track the changes in detector properties at a more precise level than before. Although we primarily focus on the Run 13 data we also analyzed

[*]dmitry.kalinkin@gmail.com
[†]d.s@plexoos.com

the data from α-calibration runs in Run 12. The same analysis procedure was performed on Run 12 data as well (see Appendix A). Because alpha runs weren't taken as frequently during Run 12, resulting plots for it don't have as much statistics as the plots for Run 13. The analysis of the data was performed with the `cnipol` package [1].

2.1 Energy calibration with α-particles

In order to perform a polarization measurement we need to measure the energy of the slow carbon ions coming from the fixed target. The calorimetry is done by utilizing the silicon strip detectors introduced above. We observe that signals coming from the detectors have the same shape. Thus each signal can be parametrized with only one parameter. We use that parameter to reconstruct the energy of the recoil particle. As of Run 2013 the data from pCarbon polarimeters comes in a form of a two quantities: the maximum amplitude and the total charge (i.e. integral). On the contrary, H-Jet data comes in full waveforms. In agreement with signals affinity, we observe a very good correlation between the maximum amplitude and the integral of the collected charge. Our choice of the former is only set by convention. For the energy calibration purposes we use low intensity ^{241}Am and ^{148}Gd radioactive sources emitting α-particles with fixed energies of $E_{\mathrm{Am}} = 5.486$ MeV and $E_{\mathrm{Gd}} = 3.183$ MeV[2] respectively. The sources are put inside the vacuum of the beam pipe in the direct acceptance of the detectors. In 2012 and 2013 two polarimeters, Y1D and B1U (see Figure 3), were supplied with ^{241}Am sources only, while the other two, Y2U and B2D, had, in addition, ^{148}Gd sources installed inside the polarimeter chambers. Prior to 2012 only the americium sources were available for calibration.

The energy of the α-particles is few times higher than that of the carbon ions reaching the detectors. We reduce the output signal by means of attenuators by a factor of five to bring it back to the range where the amplitude can be digitized by the readout electronics. In the absence of the beam we observe clean peaks from the radioactive sources as shown in Figure 17a. The peaks positions are determined using a gaussian function fit.

The current offline analysis is only based on a calibration with the ^{241}Am source. The nominal detector gain g_{Am} is defined as a ratio of the peak position, μ_{Am}, to the E_{Am} energy. This definition completely ignores possible energy losses before the sensitive detector region. This limitation can be overcome to some extent by using a second α-source. With two sources the slope of a linear calibration curve effectively takes into account the unresponsive region of the detector as illustrated with a sketch in Figure 1. This region is referred to as the *dead layer*, and we discuss it in the next section.

Figure 4 shows how the americium gain g_{Am} developed in time for all four p-Carbon polarimeters. From this we conclude that overall gain was stable on a monthly scale with only few detectors showing up to 20% instabilities in the gain. We also confirm an overall stability by looking at the ratio of the gain estimate for the polarimeters with an additional ^{148}Gd source. These quantities as a function of time are shown on Figure 5.

2.2 Effective dead layer

In our current model of the silicon detector the incident particles are assumed to pass through a region where the detector has zero response as a calorimeter, i.e. the dead layer. Adding a gadolinium alpha source to the setup allows us to put one more calibration point on our calibration curve (see Figure 1). With the points corresponding to the americium and gadolinium sources we can estimate the thickness of this layer.

The energy where the linear fit intersects the horizontal axis gives us an estimate for the initial energy of incident α-particles which would deposit all of their energy in the dead layer.

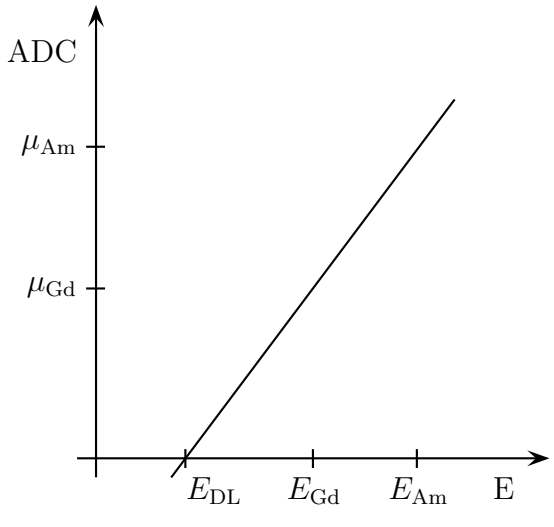

(a) Missing energy E_{DL} can be defined in the approximation of energy deposition independent of the particle energy.

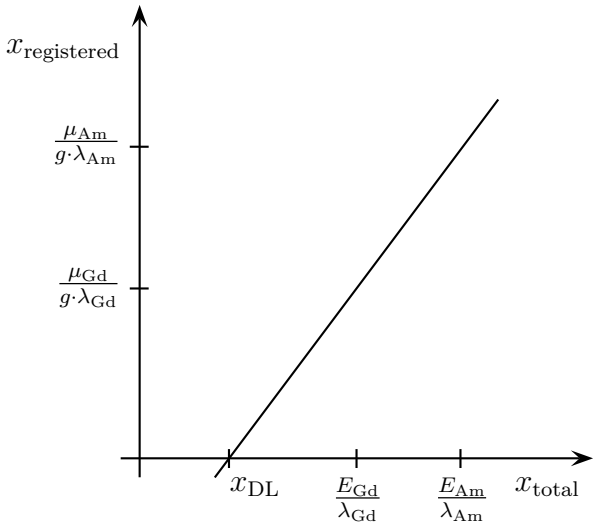

(b) Dead layer size x_{DL} is a difference between the distance that particle traveled trough the matter x_{total} and a distance on which the deposited energy was being registered by the detector $x_{\mathrm{registered}}$. Gain relation $g = g_{\mathrm{Am}} = g_{\mathrm{Gd}}$ is assumed. The linear regression gives us Equation (3). Note that the result does not depend on the value of gain g.

Figure 1: Definition of E_{DL} and x_{DL} in terms of linear regression over two points corresponding to two alpha sources.

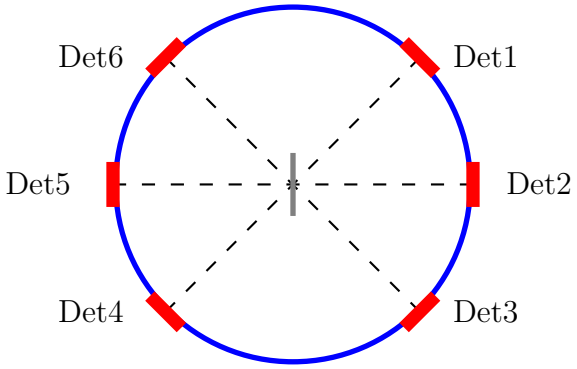

Figure 2: Schematic view of the detector alignment in the plane perpendicular to the beam. Carbon strip target is aligned vertically, detectors are aligned at angles 45°, 90°, 135° to it. The beam points into the figure perpendiculary.

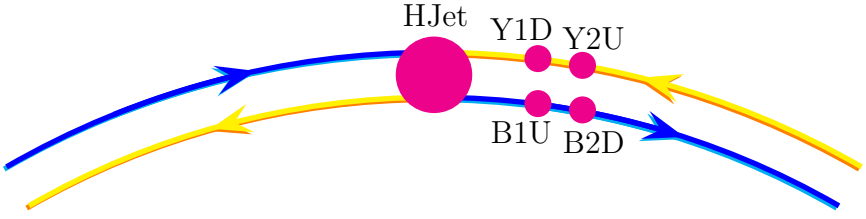

Figure 3: Schematic view of polarimeters placement around IP12.

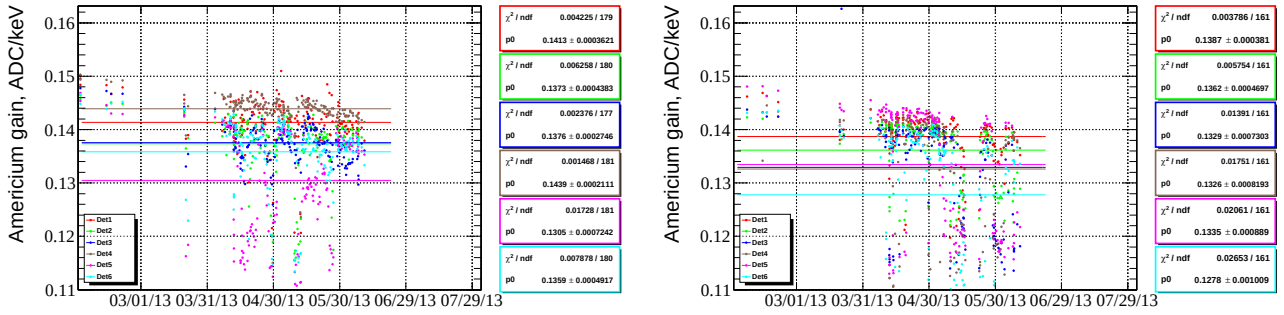

(a) B1U

(b) Y1D

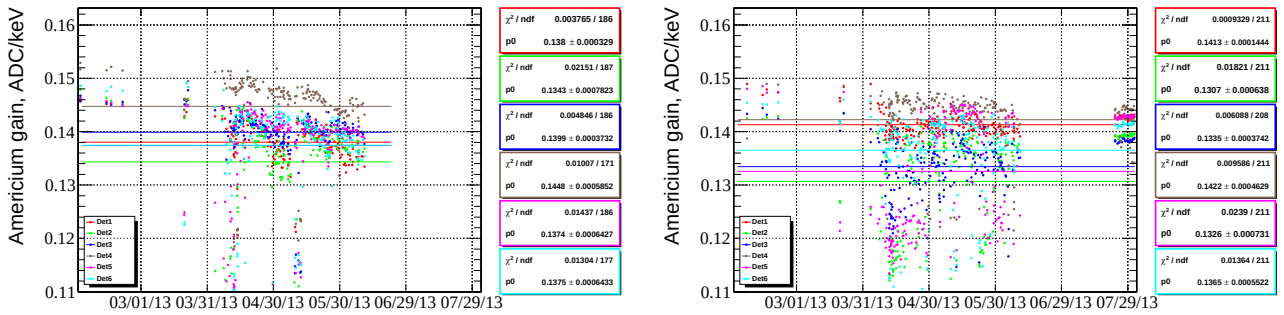

(c) B2D

(d) Y2U

Figure 4: Time dependence of the detector gain g_{Am} as measured with α-particles emitted by the ^{241}Am source. Colors represent individual detectors.

While this quantity by itself can be used to monitor the stability of the effective dead layer over time, we also present the result in $\mu g/cm^2$. For the latter, we assume that the detector response to the both incident energies is the same, and we write:

$$\frac{\mu_{Am}}{E_{Am} - E_{Am}^{\mathrm{DL}}} = \frac{\mu_{Gd}}{E_{Gd} - E_{Gd}^{\mathrm{DL}}}, \tag{1}$$

where μ_{Am} and μ_{Gd} are the mean values of the alpha peaks measured in ADC units, E_{Am} and E_{Gd} are the incident energies of α-particles, and E_{Am}^{DL} and E_{Gd}^{DL} are the energy losses in the dead layer for the respective alpha sources.

The rate at which α-particles loose their energy in the detector changes with the penetration depth. The value of stopping power can be easily derived from the *CSDA range*[1] values available at the ASTAR Database[3].

The original CSDA range data for α-particles is displayed in Figure 6a. If we take CSDA range value for the $E = E_{\mathrm{Am}}$ and $E = E_{\mathrm{Gd}}$ we will get maximal penetration depths z^0_{Am}, z^0_{Gd}. Penetration depth is then calculated as $z_i = z^0_i - \mathrm{CSDA\ range}$. Stopping power $-\frac{dE}{dz_i}$ can be then derived from E vs z_i points using simple numerical differentiation formula $\frac{df}{dx} = (f_{i+1} - f_i)/(x_{i+1} - x_i)$. The resulting plot for stopping power versus penetration depth can be seen in Figure 6b. This plot is consistent with the other plot[4] of the same dependency, derived from the data from the same ASTAR Database, but using a different method.

[1]The *CSDA range* is a very close approximation to the average path length traveled by a charged particle as it slows down to rest, calculated in the continuous-slowing-down approximation. In this approximation, the rate of energy loss at every point along the track is assumed to be equal to the total stopping power. Energy-loss fluctuations are neglected. The CSDA range is obtained by integrating the reciprocal of the total stopping power with respect to energy. – ASTAR Appendix: Significance of Calculated Quantities

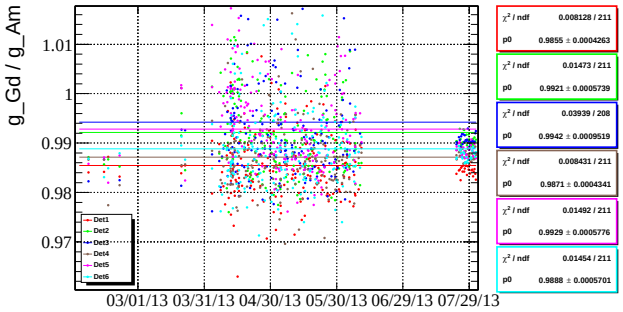

(a) Time dependence of the ratio of the gains, $g_{\mathrm{Gd}}/g_{\mathrm{Am}}$, independently measured with ^{148}Gd and ^{241}Am sources for **Y2U** polarimeter.

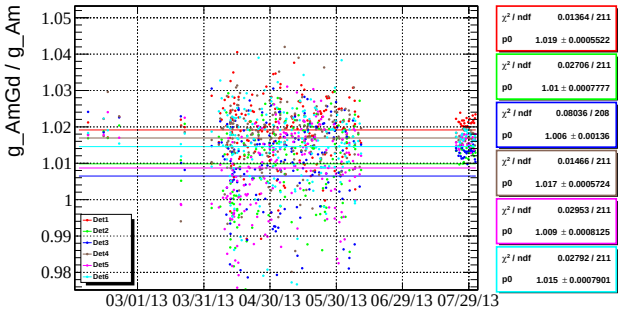

(b) Time dependence of the ratio of the gain measured with both ^{241}Am and ^{148}Gd sources to the nominal gain measured with only the ^{241}Am source for **Y2U** polarimeter.

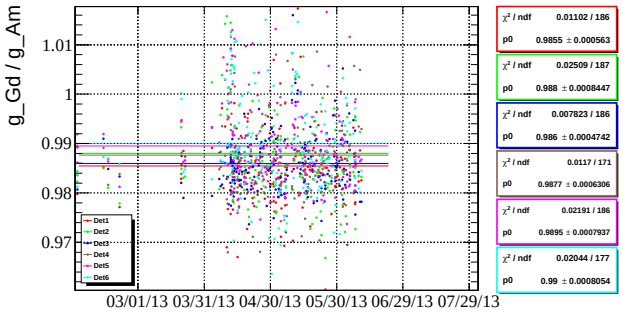

(c) Time dependence of the ratio of the gains, $g_{\mathrm{Gd}}/g_{\mathrm{Am}}$, independently measured with ^{148}Gd and ^{241}Am sources for **B2D** polarimeter.

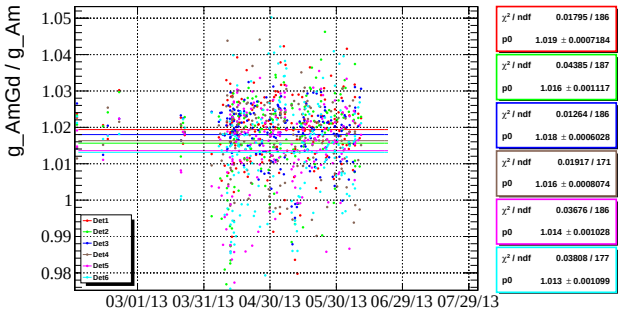

(d) Time dependence of the ratio of the gain measured with both ^{241}Am and ^{148}Gd sources to the nominal gain measured with only the ^{241}Am source for **B2D** polarimeter.

Figure 5: Comparison of the effective detector gains calculated with either one or both α-sources for the polarimeters equipped with two alpha sources. Colors represent individual detectors.

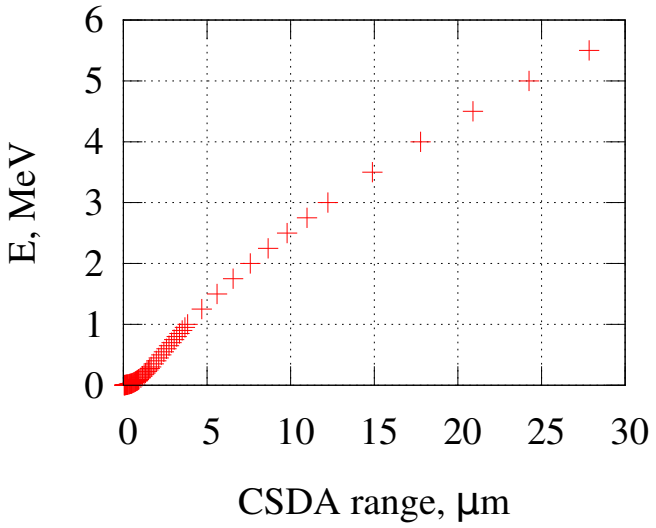

(a) CSDA versus alpha particle energy

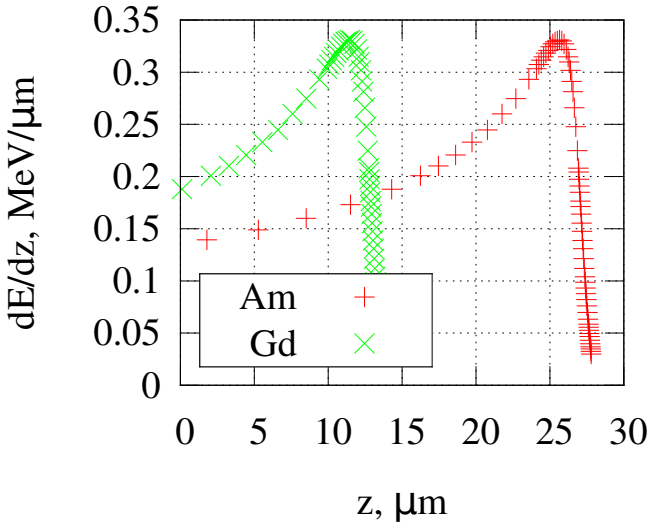

(b) Stopping power versus penetration depth

Figure 6

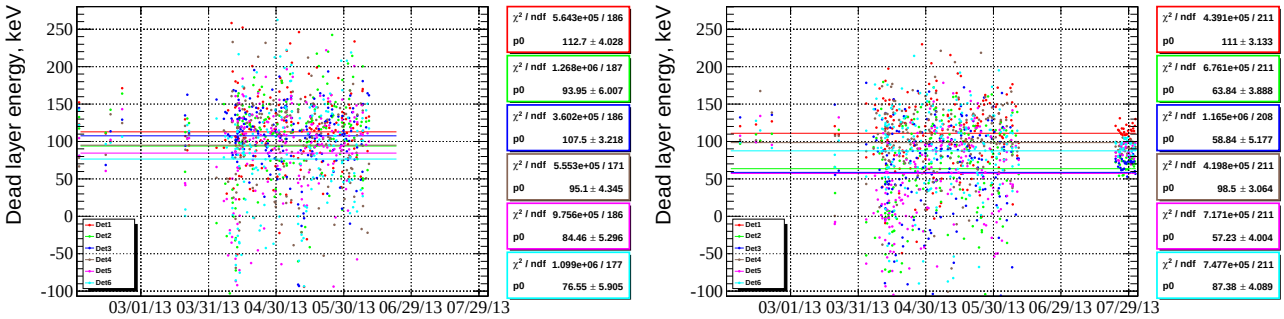

(a) B2D (b) Y2U

Figure 7: E_{DL} (see Figure 1a) is the missing energy value extracted from linear fit of the americium and gadolinium points.

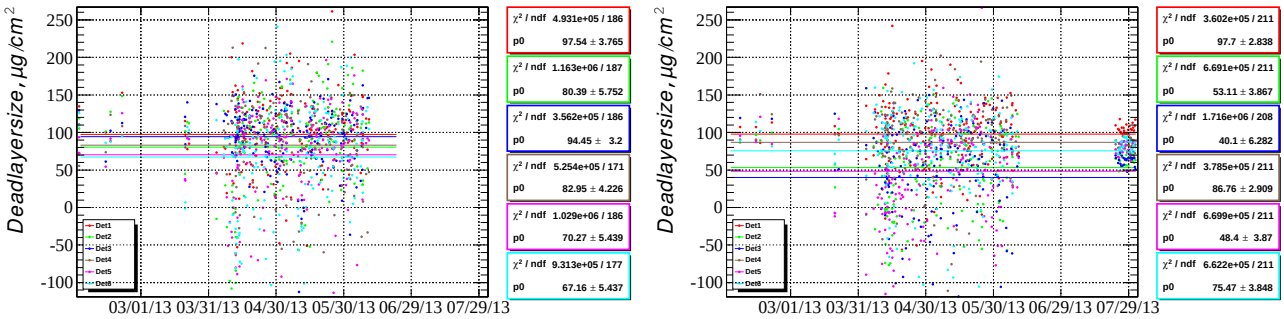

(a) B2D (b) Y2U

Figure 8: x_{DL} is the effective dead layer thickness calculated using formula (3).

As the dead layer is relatively thin (less than 1 μm) α-particles do not loose a significant fraction of their initial energy and the stopping power is approximately constant over this range. With a linear approximation for the total losses we have:

$$E_{\mathrm{Am}}^{\mathrm{DL}} \simeq x_{\mathrm{DL}}\lambda_{\mathrm{Am}} \qquad E_{\mathrm{Gd}}^{\mathrm{DL}} \simeq x_{\mathrm{DL}}\lambda_{\mathrm{Gd}} \tag{2}$$

with values for the stopping power $\lambda_{\mathrm{Am}} = 140$ keV/μm and $\lambda_{\mathrm{Gd}} = 190$ keV/μm taken from the plot on Figure 6b at $z = 0$. Combining Equations (1) and (2) we obtain the following formula for the size of the effective dead layer:

$$x_{DL} = \frac{\mu_{Gd}E_{Am} - \mu_{Am}E_{Gd}}{\mu_{Gd}\lambda_{Am} - \mu_{Am}\lambda_{Gd}} \tag{3}$$

This formula could be also realized as a linear regression fit of the plot at Figure 1b.

The thickness of the dead layer thus extracted from the all available calibration runs in Run 13 are shown in Figure 8. The average size of the effective dead layer is estimated to be within 80 to 100 $\mu g/cm^2$.

2.3 Bias current

In Figures 5, 7 and 8 there are few measurements taken before and after run13. When comparing these measurements with the measurements taken during the run we see that later are showing

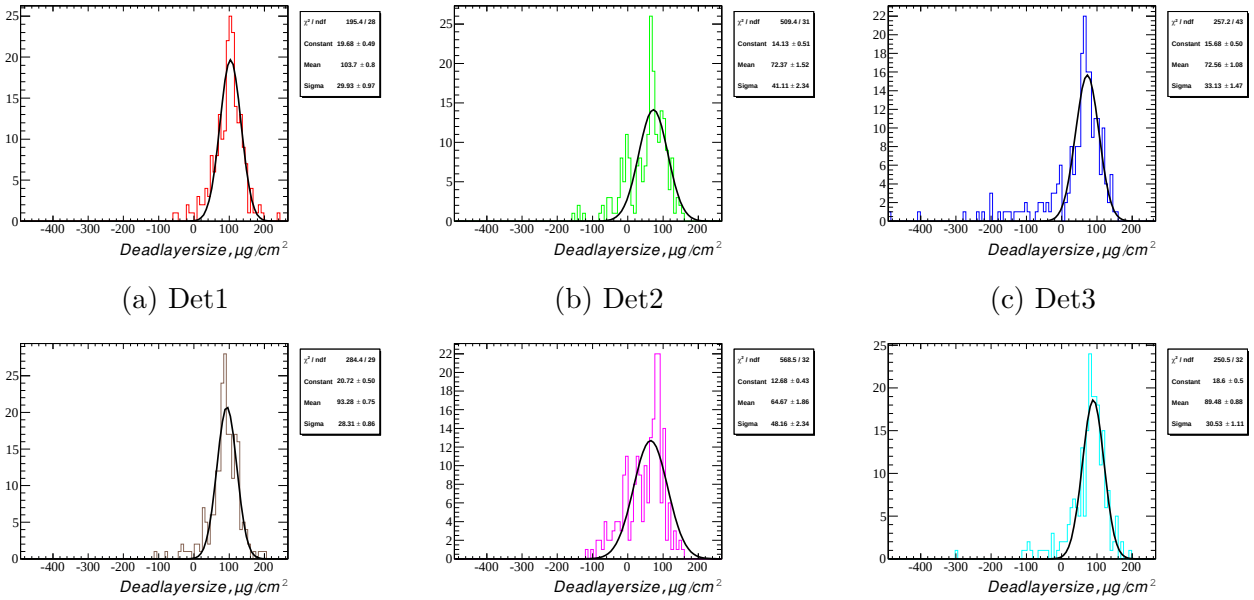

(a) Det1 (b) Det2 (c) Det3

(d) Det4 (e) Det5 (f) Det6

Figure 9: x_{DL} distribution in the measurements for Y2U.

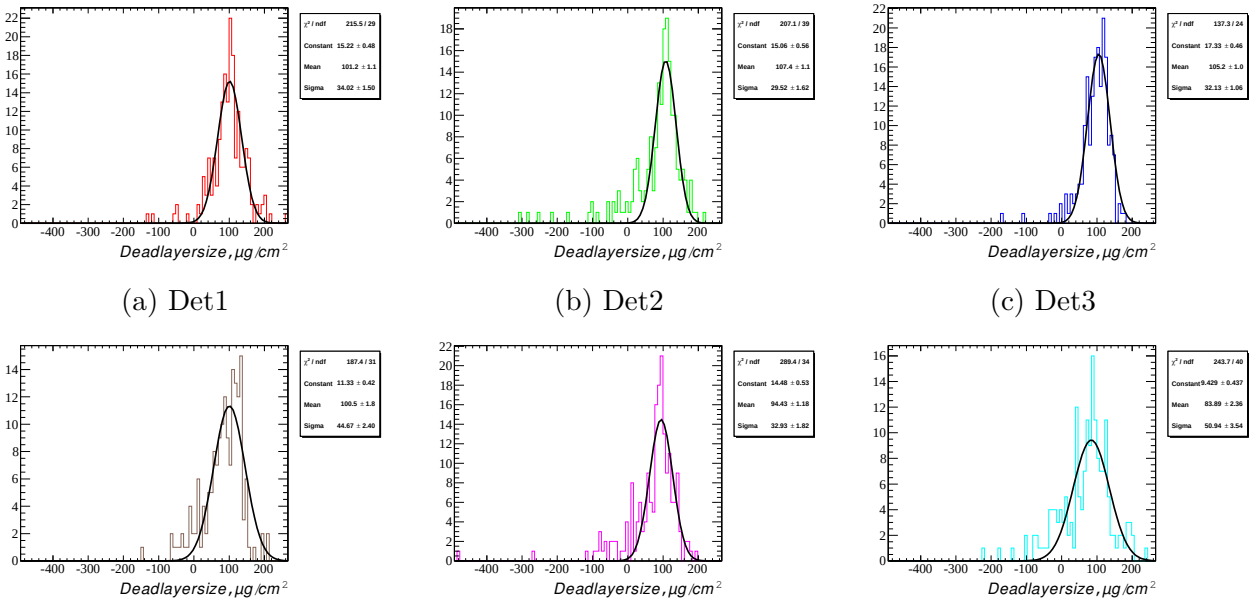

(a) Det1 (b) Det2 (c) Det3

(d) Det4 (e) Det5 (f) Det6

Figure 10: x_{DL} distribution in the measurements for B2D.

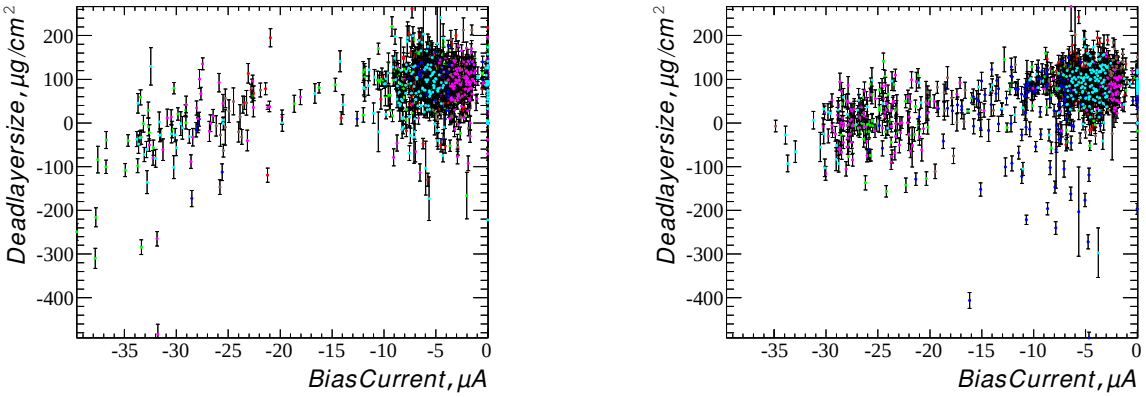

(a) B2D

(b) Y2U

Figure 11: Bias current versus dead layer size dependency.

much higher spread. We investigate this abnormality by looking at correlations with other detector work parameters.

One of the work parameters of our silicon detector that we measure is a bias current – current constantly flowing through detector (in this case – set of 12 strips). Current was measured for each of the six silicon detectors on all polarimeters, measurements were taken each five minutes. Values lie mostly in range from -30 to 0 μA. It was interesting to see how this current affects calibration characteristics of our detector. For example, it is known that higher bias voltage should decrease size of depleted zone, i.e. decrease size of effective dead layer. On our plots (Figure 11) we see some weak correlation between effective dead layer size and bias current.

Much stronger correlation is seen when we compare the bias current with the gain (Figure 12). We use this correlation to produce linear model to correct our alpha gains to their values at zero bias current. The resulting plot is presented at Figure 13. Unlike original plot at Figure 13 this one shows much lower spread.

We also tried to see if the variation of the bias current correlates with the beam properties. To do that we took average of the beam intensity values at a plateau (values $> 50 \cdot 10^{11}$ protons) of the fill happened before the alpha measurement. That value was then plotted versus the bias current as shown at Figure 14.

2.4 Linearity of the amplifiers

The signal generated in the detector propagates through several stages of amplification. Linearity of the downstream amplifiers can be checked by attenuating the signal in a place on the signal path preceding the amplification, and then comparing the measured reduced amplitude with the expected one properly scaled by a known factor.

The shaper boards have a resistive divider with a multiplexer controlled by software settings. For normal polarization measurements of sub-MeV carbon ions the on-board attenuator is set to 1, i.e. no signal attenuation. During regular alpha measurements the attenuator is set to 1/5. In this study we check the other two attenuator settings of 1/10 and 1/3. The alpha peaks obtained with these attenuator settings are shown in Figure 17 and the mean values corresponding to the gaussian fits are listed in Table 1. Note that with the attenuator setting of 1/3 the americium peak ends up in the overflow bin as the events are outside of the detector dynamic range. The cumulative effect of a possible non-linearity in the amplified signal is checked by using the relation in which the mean of the peak is expected to scale with the attenuator settings:

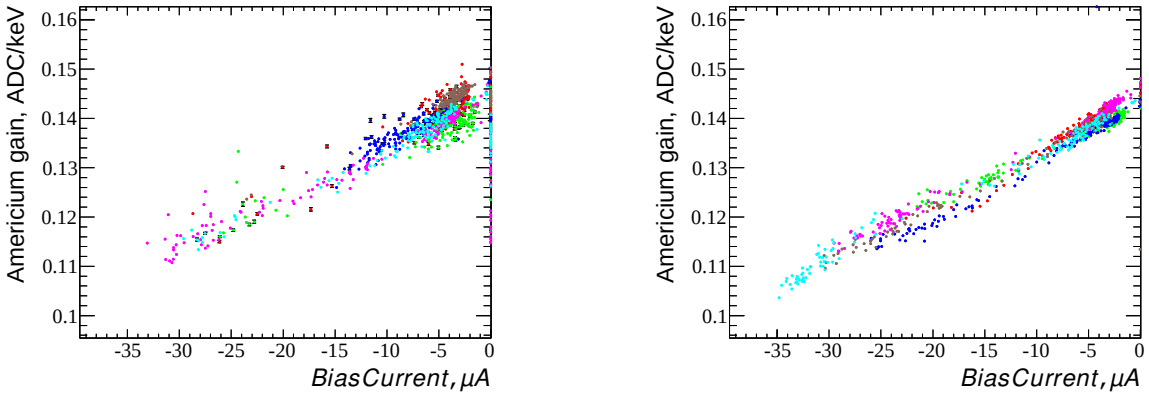

(a) B1U

(b) Y1D

(c) B2D

(d) Y2U

Figure 12: Bias current versus americium gain ($\mu_{\mathrm{Am}}/E_{\mathrm{Am}}$) dependency. The colors represent different detectors.

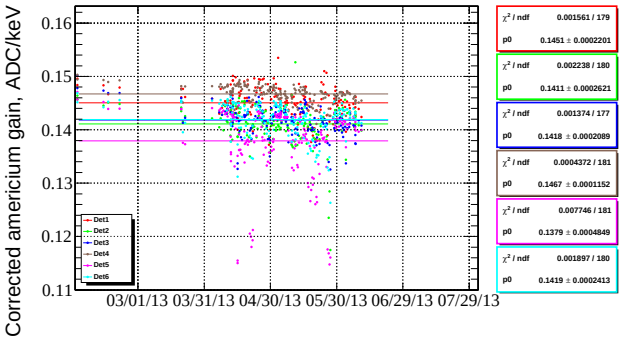

(a) B1U

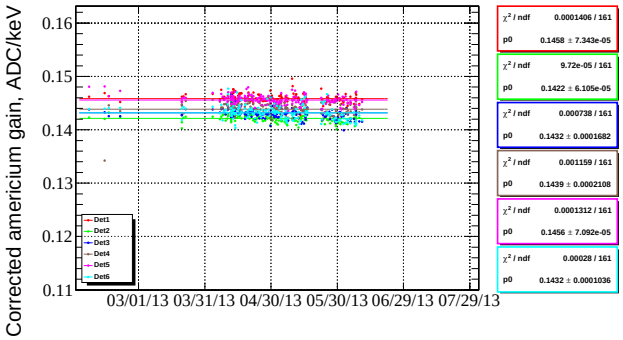

(b) Y1D

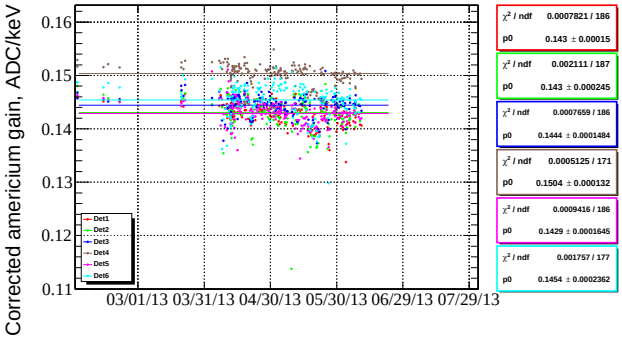

(c) B2D

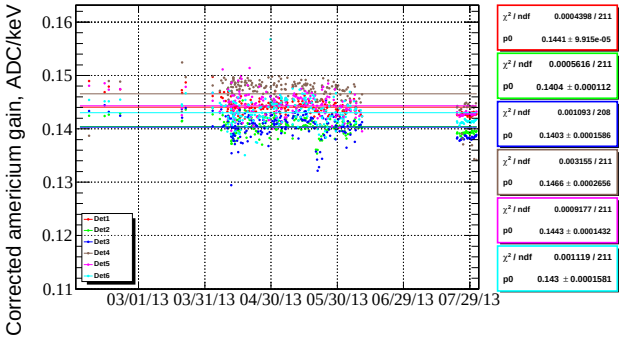

(d) Y2U

Figure 13: Time dependence of the detector gain g_{Am} that was corrected to zero bias current using the slope from Figure 12.

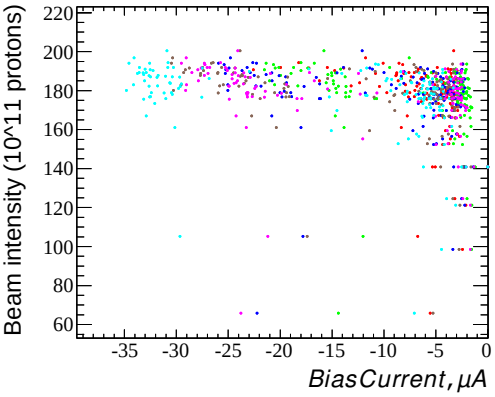

(a) Y1D

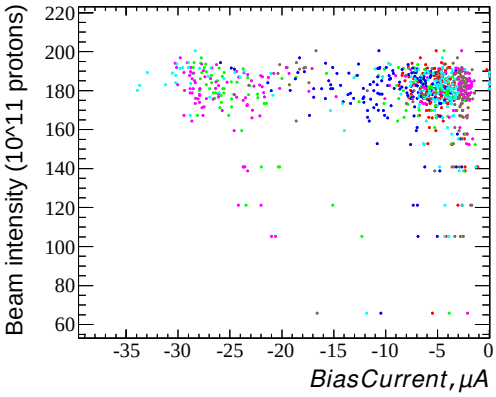

(b) Y2U

Figure 14: The average bias current during an alpha measurement versus the average beam intensity in the preceding store. The colors represent different detectors.

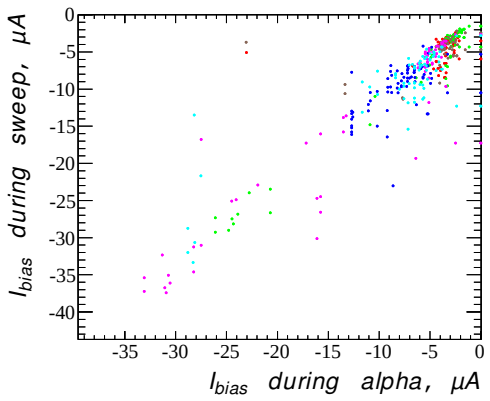

(a) B1U

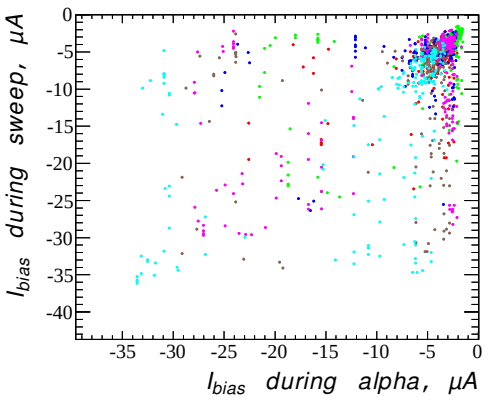

(b) Y1D

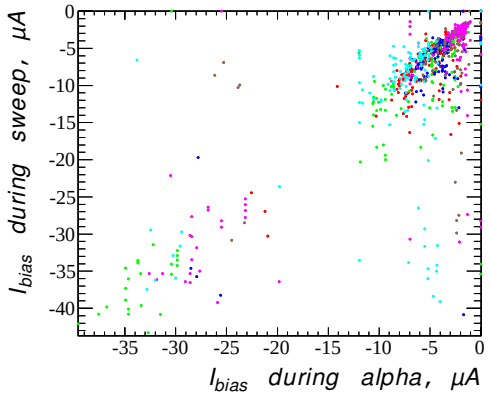

(c) B2D

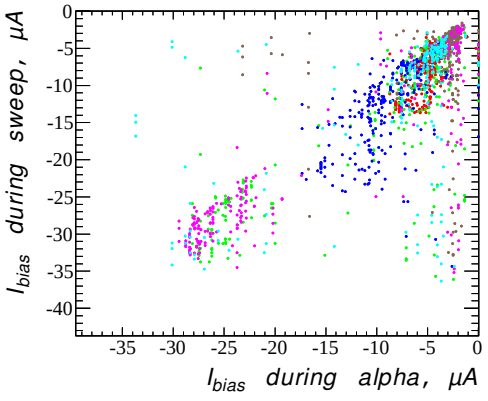

(d) Y2U

Figure 15: Correlation between the mean bias current during the alpha measurements and bias currents that were taken during the sweep measurements.

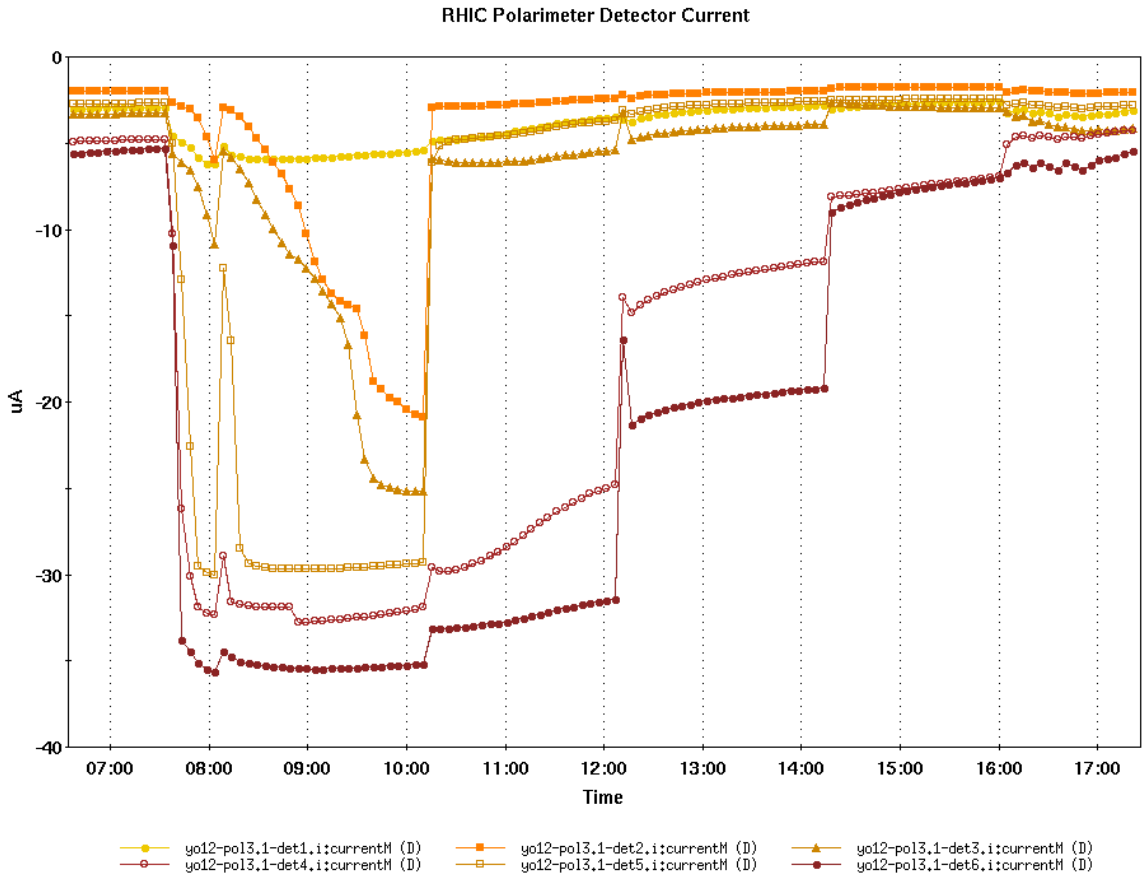

Figure 16: Bias current variation in Y1D detector during fill 17384. Some jumps coincide with polarization measurements.

$$\lambda_1/\lambda_2 = \mu_1/\mu_2. \tag{4}$$

Table 1: The mean positions of the ^{241}Am and ^{148}Gd α-peaks with different attenuator settings.

Attenuation λ	Alpha Run Id	Am Mean, ADC	Gd Mean, ADC
$\frac{1}{10}$	atten_1_over_10.yel2.alpha0	77.0 ± 0.7	44.2 ± 0.4
$\frac{1}{5}$	13_310713.yel2.alpha0	154.9 ± 2.7	88.9 ± 1.5
$\frac{1}{3}$	atten_1_over_3.yel2.alpha0	—	149.4 ± 2.5

This effect relative to one of the attenuator settings can be defined as $\Delta l = \frac{\lambda_1\mu_2}{\lambda_2\mu_1} - 1$. For the three pairs of measurements we calculate very small deviations from the linear Equation (4).

$$\frac{154.9}{77.0 \times 2} - 1 = 0.6\% \qquad \frac{88.9}{44.0 \times 2} - 1 = 0.6\% \qquad \frac{149.4 \times 3}{88.9 \times 5} - 1 = 0.8\% \tag{5}$$

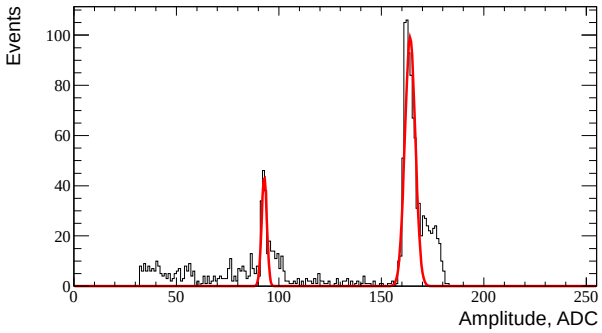

(a) Signal attenuated to 1/5

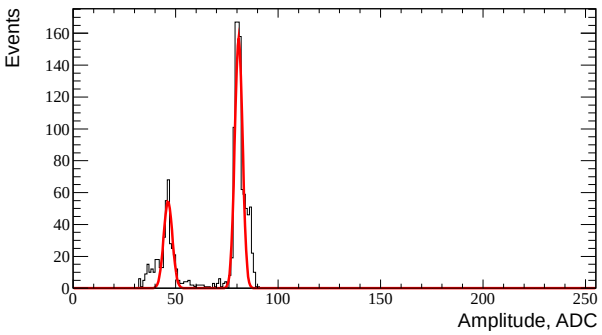

(b) Signal attenuated to 1/10

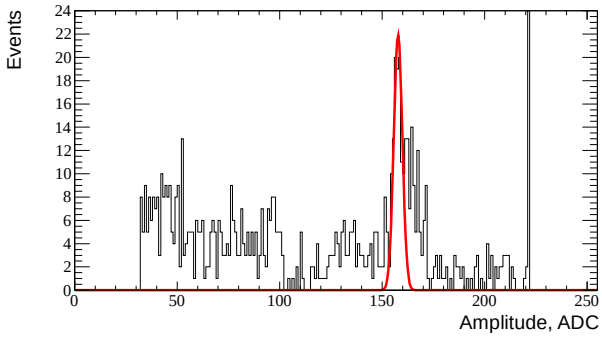

(c) Signal attenuated to 1/3

Figure 17: Alpha peaks as seen with different on-board attenuator settings (Y2U).

3 Implementing the bias current correction

Alpha gain is an important quantity that is used in processing sweep polarization measurements to convert ADC values to the energy scale. Each sweep measurement has an assigned alpha measurement from which alpha gain value is taken from. When looking at available alpha measurements, we observe a strong correlation between the gain and the detector bias current. We can assume that the same gain dependency is also held for regular polarization measurements. The later is in agreement with observation of carbon gains vs bias current calibration

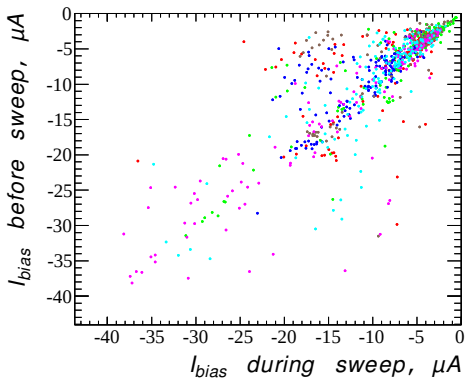

(a) B1U

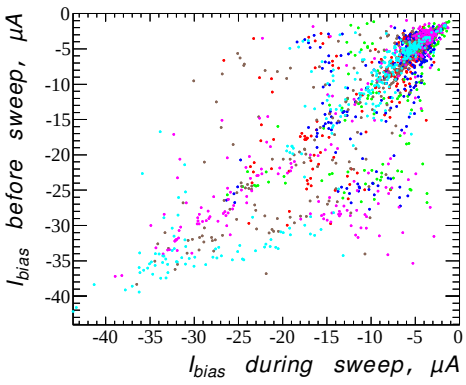

(b) Y1D

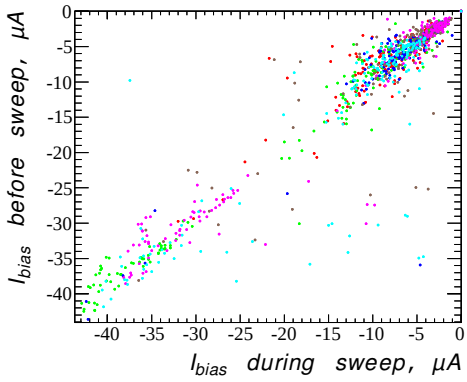

(c) B2D

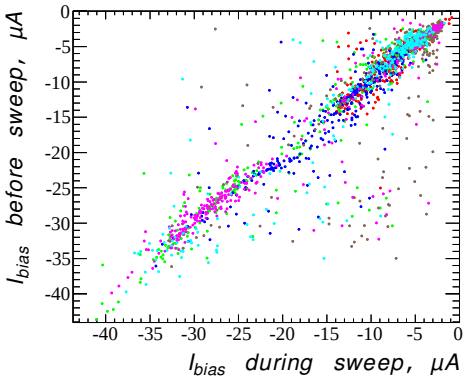

(d) Y2U

Figure 18: Correlation of bias currents that fall in time windows [starttime, endtime] and [starttime − 5 min, starttime].

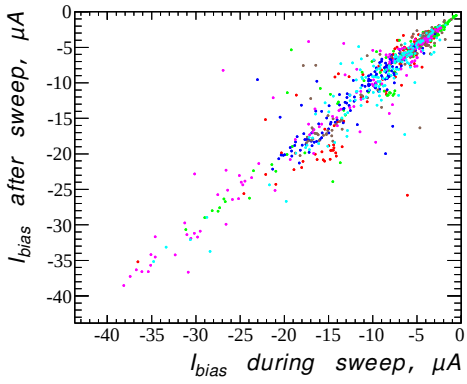

(a) B1U

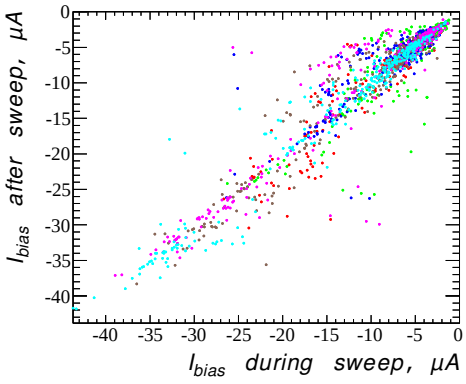

(b) Y1D

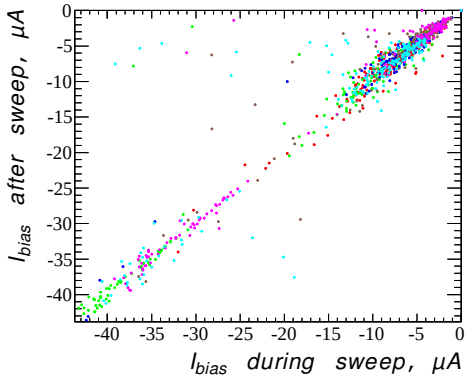

(c) B2D

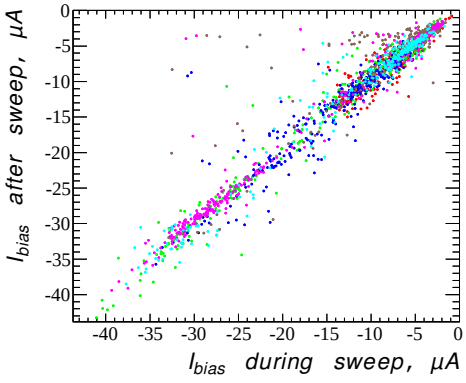

(d) Y2U

Figure 19: Correlation of bias currents that fall in time windows [starttime, endtime] and [endtime, endtime + 5 min].

[5][6]. It is also known that bias currents can vary drastically during the fill (Figure 16). This suggests that an effective gain value in the sweep measurement may differ from the it's value in corresponding alpha measurement, if bias current changed between those two measurements. This variation may go as high as $\approx 20-40\%$ on the operational bias current span (Figure 12). Knowing bias current during sweep and alpha measurement one can apply a correction to alpha gain to obtain an effective gain for the sweep measurement.

The main problem that one faces when implementing the correction is the low bias current sampling rate. For the most of the run 13 the period of these measurements was equal to 5 minutes. At the same time the most common polarization measurement – sweep measurement normally takes no more than a couple minutes. Because of that there is a big chance that for many polarization measurements there will be no bias current measurement taken during them. To overcome this we must soften our criteria of timewise selection of the appropriate bias current measurement. In our study we evaluated two schemes:

1. Extending the query window backward in time.

2. Extending the query window forward in time.

To study option 1 we looked at correlation between bias current measurement taken during the sweep measurements (where available) with the previous measurement (Figure 18). For option 2 the correlation has been plotted against next available measurement (Figure 19). The correlation for the later option show lower spread. In other words, the value bias current during the sweep measurement is closer to it's value right after the measurement than to the value right before it. For our purposes we prefer the value that is closer to the value during the sweep measurement, so we extend bias current query window forward in time. In our particular implementation we query bias current values in the time window $[\text{starttime}, \max(\text{endtime}, \text{starttime} + 500 \text{ sec})]$ (starttime and endtime denote measurement's start and end timestamps). That way our query window is never less than 8.3 minutes and always contains at least one bias current measurement.

In our approach we utilize following correction formula:

$$g_{\text{sweep}} = g_{\text{alpha}} + \frac{dg}{dI}(I_{\text{sweep}} - I_{\text{alpha}}) \tag{6}$$

where $\frac{dg}{dI}$ is a slope taken from linear fit of correlation from Figure 12 for the detector, I_i, g_i – apropriate bias currents and gains for the channel. In current implementation this calculation is split in two steps: First, when processing alpha measurements channel calibration, we calculate gain corrected to zero bias current as $g_{I=0} = g_{\text{alpha}} - \frac{dg}{dI} I_{\text{alpha}}$ and store it into `fZeroBiasGain` field of channel's `ChannelCalib` structure. Second, when processubg sweep measurement, we continue calculation on the calibration set inherited from alpha file processing step and obtain our effective gain as $g_{\text{sweep}} = g_{I=0} + \frac{dg}{dI} I_{\text{sweep}}$, storing it in the `fEffectiveGain` field for subsequent use in event processing. For more implementation details see [8].

4 Conclusions

Based on the analysis presented in this note we establish that the changes in the bias currents in our silicon detectors heavily depend on the beam activity in RHIC. At the moment, we do not see that the bias current correlates with the beam intensity (Figure 14) but in further studies we plan to investigate if other beam or machine parameters have direct impact on the detectors.

We observed noticeable changes in detector bias current during fills of run 13. These changes affected detector gain values and lead to a mismatch between gain value measured during

calibration and effective gain during polarization measurements. A correction based for this effect was implemented in the analysis code to be applied in run 13 analysis (see Section 3).

The presence of the two α-sources in the polarimeters allowed us to find a correction for the effective detector gain by taking into account dead layer energy losses. We find this correction (Figure 5) to be at $\approx 5\%$ level with respect to the nominal calibration procedure with one radioactive source. In addition, we estimate the thickness of the effective dead layer to be $\approx 80\ \mu g/cm^2$. This number disagrees with the value extracted from the nominal "banana" fit to the carbon data where the effective dead layer is estimated to be $\approx 35\ \mu g/cm^2$ and the value of 1500 Å ($\approx 35\ \mu g/cm^2$) provided by instrumentation group. A possible explanation for this discrepancy is that we overestimate the effective dead layer thickness as measured with α-particles by not taking into account the extra material of the protective coating of the alpha source.

Comparing the detector gains measured before and after the beam time we conclude that there was no significant radiation damage of the detectors.

A similar study has been performed for the 2012 data. The corresponding plots can be found in Appendix A.

A Appendix: Run12 plots

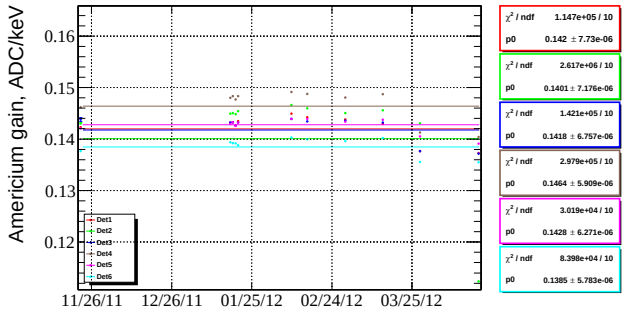

(a) B1U

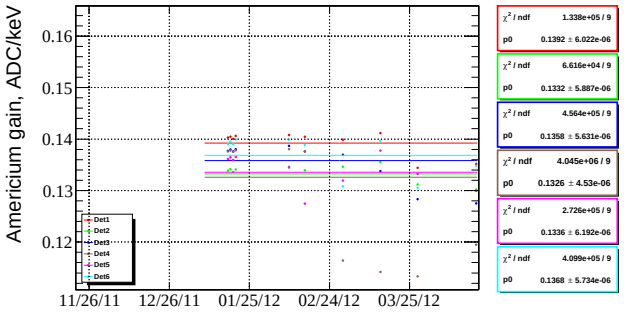

(b) Y1D

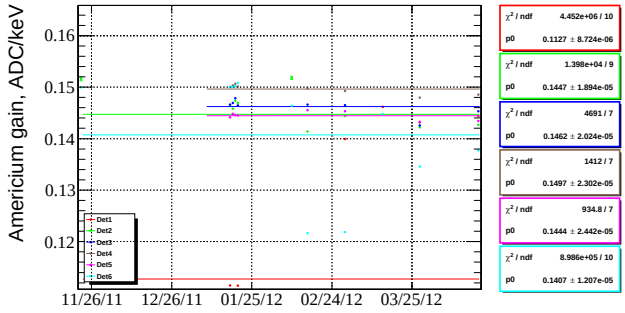

(c) B2D

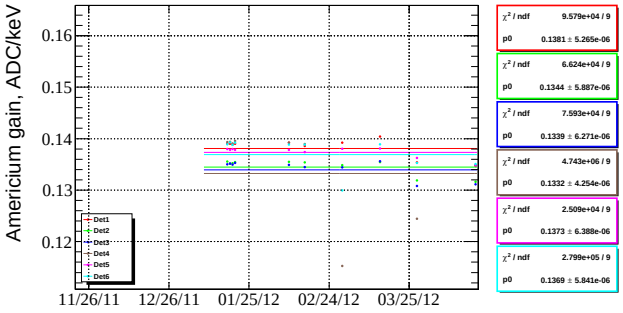

(d) Y2U

Figure 20: Time dependence of the detector gain g_{Am} as measured with α-particles emitted by the ^{241}Am source. Colors represent individual detectors. (run12_alpha)

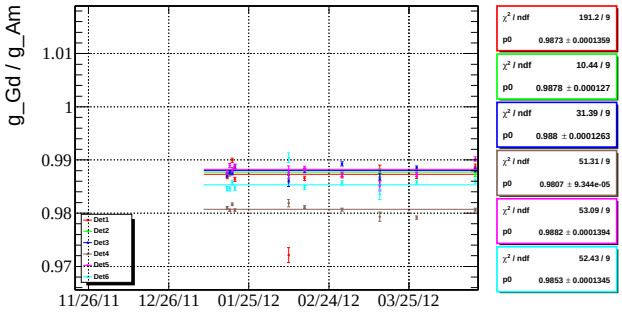

(a) Relation of gadolinium and americium gains for **Y2U** polarimeter.

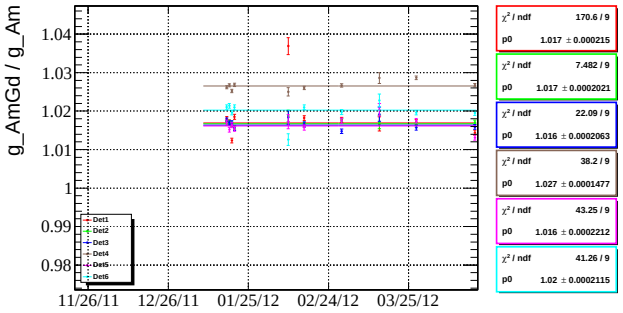

(b) Relation of two-point (americium and gadolinium) linear fit slope and americium gain for **Y2U** polarimeter.

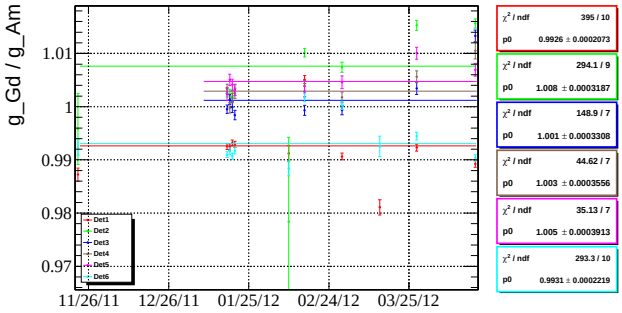

(c) Relation of gadolinium and americium gains for **B2D** polarimeter.

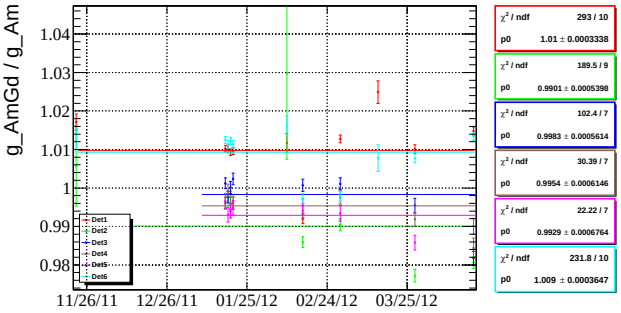

(d) Relation of two-point (americium and gadolinium) linear fit slope and americium gain for **B2D** polarimeter.

Figure 21: Comparison of the effective detector gains calculated with either one or both α-sources for the polarimeters equipped with two alpha sources. Colors represent individual detectors. (run12_alpha)

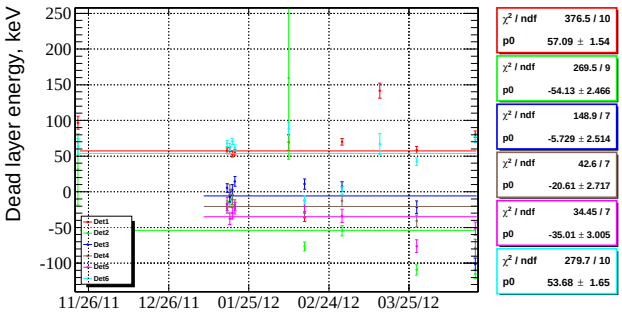

(a) B2D

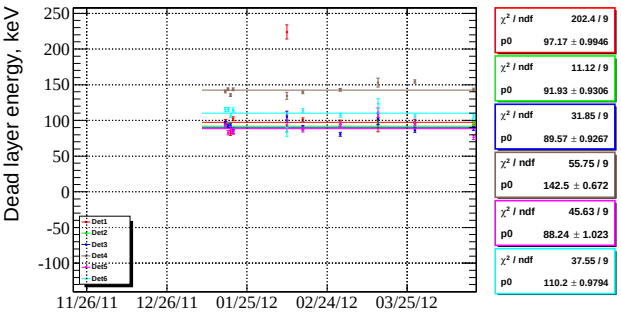

(b) Y2U

Figure 22: E_{DL} (see Figure 1a) is the missing energy value extracted from linear fit of the americium and gadolinium points. (run12_alpha)

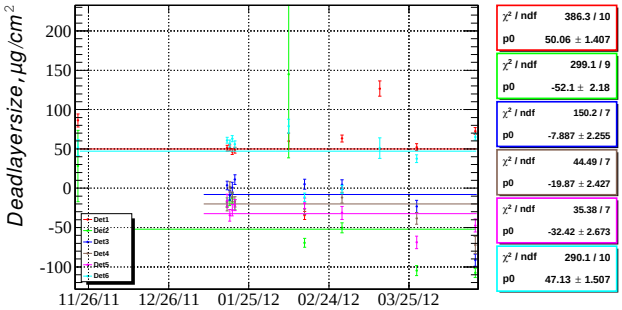

(a) B2D

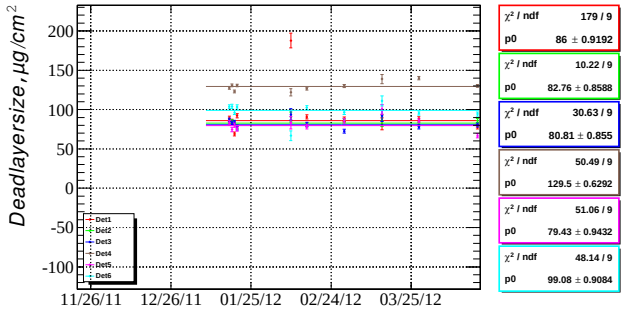

(b) Y2U

Figure 23: x_{DL} is the effective dead layer thickness calculated using formula (3). (run12_alpha)

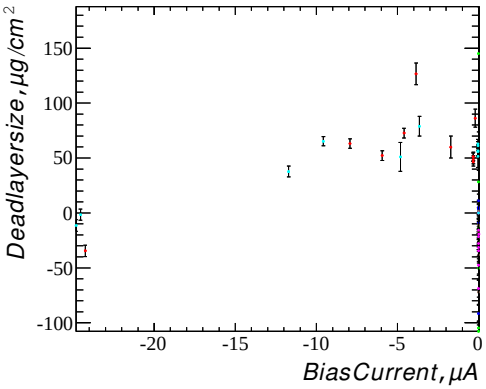

(a) B2D

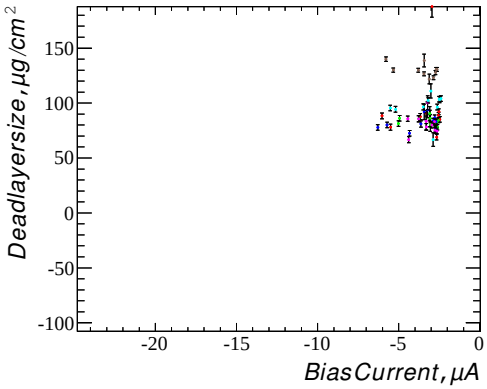

(b) Y2U

Figure 24: Bias current versus dead layer size dependency. (run12_alpha)

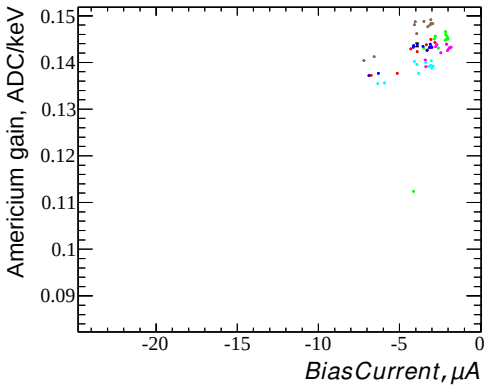

(a) B1U

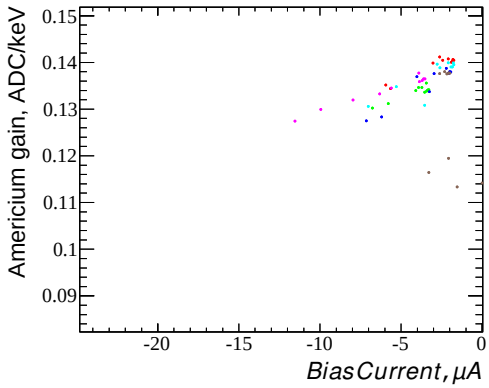

(b) Y1D

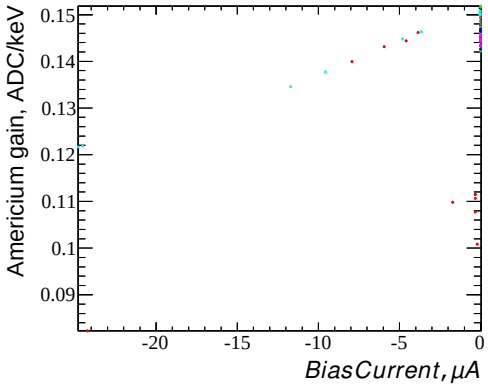

(c) B2D

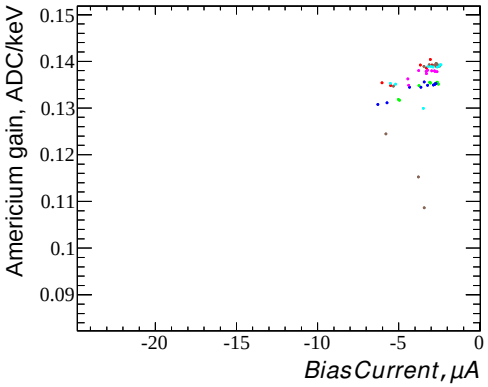

(d) Y2U

Figure 25: Bias current versus americium gain ($\mu_{\mathrm{Am}}/E_{\mathrm{Am}}$) dependency. The colors represent different detectors. (run12_alpha)

References

[1] RHIC polarimetry analysis framework: https://github.com/rhicspin/cnipol

[2] A. Rytz, *At. Data and Nucl. Data Tables* **47**, 205 (1991).

[3] ASTAR database. Stopping power and range tables for helium atoms: http://physics.nist.gov/PhysRefData/Star/Text/ASTAR.html

[4] B. Schmidke, *Carbon & alpha E-deposition in Si*, July 8 (special meeting) https://wiki.bnl.gov/rhicspin/upload/7/72/Schmidke_Special_meeting_08.07.13.pdf

[5] B. Schmidke, *Alpha gain* $\leftrightarrow$ *carbon gain*, August 16 (special meeting) https://wiki.bnl.gov/rhicspin/upload/f/fe/Schmidke_Special_meeting_16.08.13.pdf

[6] D. Kalinkin, *Carbon gain vs. Ibias* (see slide 7), August 16 (special meeting) https://wiki.bnl.gov/rhicspin/upload/5/5f/Dkalinkin_16-08-13.pdf

[7] RHIC polarimetry results: http://www.phy.bnl.gov/cnipol/rundb/

[8] D. Kalinkin, commit `848ceac4dcc15b2805552b721f033b9d3852e0f6` in cnipol repository https://github.com/rhicspin/cnipol/commit/848ceac4d